

## Southern Ocean Climate and Sea Ice Anomalies Associated with the Southern Oscillation

R. KWOK

*Jet Propulsion Laboratory, California Institute of Technology, Pasadena, California*

J. C. COMISO

*NASA Goddard Space Flight Center, Greenbelt, Maryland*

(Manuscript received 5 February 2001, in final form 7 August 2001)

### ABSTRACT

The anomalies in the climate and sea ice cover of the Southern Ocean and their relationships with the Southern Oscillation (SO) are investigated using a 17-yr dataset from 1982 to 1998. The polar climate anomalies are correlated with the Southern Oscillation index (SOI) and the composites of these anomalies are examined under the positive ( $SOI > 0$ ), neutral ( $0 > SOI > -1$ ), and negative ( $SOI < -1$ ) phases of SOI. The climate dataset consists of sea level pressure, wind, surface air temperature, and sea surface temperature fields, while the sea ice dataset describes its extent, concentration, motion, and surface temperature. The analysis depicts, for the first time, the spatial variability in the relationship of the above variables with the SOI. The strongest correlation between the SOI and the polar climate anomalies are found in the Bellingshausen, Amundsen, and Ross Seas. The composite fields reveal anomalies that are organized in distinct large-scale spatial patterns with opposing polarities at the two extremes of SOI, and suggest oscillations that are closely linked to the SO. Within these sectors, positive (negative) phases of the SOI are generally associated with lower (higher) sea level pressure, cooler (warmer) surface air temperature, and cooler (warmer) sea surface temperature in these sectors. Associations between these climate anomalies and the behavior of the Antarctic sea ice cover are evident. Recent anomalies in the sea ice cover that are clearly associated with the SOI include the following: the record decrease in the sea ice extent in the Bellingshausen Sea from mid-1988 to early 1991; the relationship between Ross Sea SST and the ENSO signal, and reduced sea ice concentration in the Ross Sea; and the shortening of the ice season in the eastern Ross Sea, Amundsen Sea, far western Weddell Sea and lengthening of the ice season in the western Ross Sea, Bellingshausen Sea, and central Weddell Sea gyre during the period 1988–94. Four ENSO episodes over the last 17 years contributed to a negative mean in the SOI ( $-0.5$ ). In each of these episodes, significant retreats in ice cover of the Bellingshausen and Amundsen Seas were observed showing a unique association of this region of the Antarctic with the Southern Oscillation.

### 1. Introduction

The Southern Oscillation (SO) refers to the seesaw in the surface pressure anomalies between the Indian Ocean–Australian region and the southeastern tropical Pacific on a seasonal and interannual timescale. The large-scale character of the SO in the Tropics and subtropics in the Southern Hemisphere is well known (Philander and Rasmusson 1985). The SO has a signature that extends to the mid- and high latitudes in the Southern Hemisphere in the winter and summer. The high-latitude signature of the SO has associated anomalies over the Antarctic sea ice cover. Understanding these links between the SO and Antarctic sea ice cover are

important due to the sensitivity of sea ice to anomalies in climate forcing as sea ice interacts with the global climate over a broad range of spatial and temporal scales (Schlesinger and Mitchell 1985; Manabe et al. 1991). Sea ice albedo feedback involves changes in the climatological area of the ice cover and adjustments in the poleward heat transport by the atmosphere, in addition to changes in the thickness, albedo, and temperature of ice within the Antarctic ice pack. The ocean structure and circulation are affected during sea ice growth, as salt is rejected to the underlying ocean increasing its density and leading sometimes to deep ocean convection and bottom water formation. Equatorward transport of ice results in a net flux of freshwater and negative heat. Thus, anomalies in these polar processes have complex consequences in the global climate.

Many studies have analyzed the recent behavior of the Antarctic ice extent and have suggested connections between sea ice extent and the Southern Oscillation

---

*Corresponding author address:* Dr. R. Kwok, Jet Propulsion Laboratory, California Institute of Technology, 4800 Oak Grove Dr., Pasadena, CA 91109.  
E-mail: ron.kwok@jpl.nasa.gov

(Carleton 1988; Jacobs and Comiso 1993; Simmonds and Jacka 1995; Gloersen 1995; Ledley and Huang 1997; Jacobs and Comiso 1997; Watkins and Simmonds 2000). Using a 10-yr dataset (1985–94), White and Peterson (1996) found coupled anomalies that propagate eastward with the Antarctic Circumpolar Current during a period of 4–5 years (wavenumber 2) and taking 8–10 years to encircle Antarctica. It was suggested that this Antarctic Circumpolar Wave (ACW) is associated with ENSO-related activities in the equatorial Pacific, possibly through an atmospheric teleconnection with higher southern latitudes. Peterson and White (1998), in a case study, show ENSO can be a possible source of the interannual anomalies for sustaining the ACW in the western subtropical South Pacific. Parkinson (1998) also suggests that the lengthening/shortening sea ice season might be related to the variability of the ACW. Bonekamp et al. (1999) in an examination of the European Centre for Medium-Range Weather Forecasts (ECMWF) Atmospheric Reanalysis dataset from 1979 to 1994, however, did not find eastward propagating anomalies suggestive of an ACW prior to 1984. For that time period at least, a two-regime structure with and without the presence of ACW was indicated. Yuan and Martinson (2000) explored possible relationships between the record of Antarctic sea ice extent between 1978 and 1996 and global climate variability. Their analyses show a strong link of the sea ice edge anomalies in the Amundsen, Bellingshausen, and Weddell Seas to extrapolar climate. In a recent article, Venegas et al. (2001) found coupled oscillations in Antarctic sea ice and atmosphere in the South Pacific sector.

The objective of this study is to explore the spatial details in the teleconnections between SO and the anomalies in the Southern Ocean climate and in particular the anomalies of the Antarctic sea ice cover. Our approach is to analyze the linear correlation of the Southern Oscillation index (SOI) with the polar climate anomalies, and to examine the composites of these anomalies during three phases of the SOI that we define as  $SOI > 0$ ,  $0 > SOI > -1$ , and  $SOI < -1$ , and henceforth will be referred to as the positive, neutral, and negative phases. The datasets used here span a 17-yr period from 1982 to 1998. Our study takes advantage of new data on ice motion and ice surface temperature derived from passive microwave imagery and the National Oceanic and Atmospheric Administration's (NOAA) Advanced Very High Resolution Radiometer (AVHRR) data. Rather than having to restrict our study area to the ice edge region, as was done previously (White and Peterson 1996), this dataset allows a more detailed examination of the spatial signatures of the climate and sea ice anomalies.

The paper is composed of five sections. Section 2 describes the climate and sea ice datasets used in our analysis. Section 3 presents the spatial pattern of correlation between the Southern Ocean climate anomalies and the SOI, and the composite patterns of the climate

and sea ice anomalies associated with three phases of the SOI over 17 years. We discuss our results in the context of previous work in section 4. The paper is summarized in the last section.

## 2. Data description

### a. Climate data

The monthly SOI used in this study were those of the Climate Analysis Center. The SOI is the difference between the standardized Tahiti sea level pressure (SLP) and the standardized Darwin SLP measurements. Large negative excursions of the SOI are associated with intense El Niño–Southern Oscillation (ENSO) episodes (Fig. 1). Between 1982 and 1998, there were four ENSO episodes in 1983, 1987, 1992, and 1998 occurring at approximately the same frequency and with approximately the same duration. This can be seen in the strong 4-yr and 2.5-yr primary and secondary peaks (Fig. 1) in the spectral amplitude of the SOI time series over the 17 years between 1982 and 1998. In the analyses that follow, we use a three-month running average of the SOI to avoid a significant portion of the noise due to small-scale and transient phenomena that are not associated with the large-scale coherent SO signal.

Monthly SLP, 1000-hPa zonal and meridional geostrophic winds (ZW, MW), and surface air temperature (SAT) anomalies are computed from the National Centers for Environmental Prediction–National Center for Atmospheric Research (NCEP–NCAR) reanalysis output (Kalnay et al. 1996). The anomaly fields in the global NCEP  $2.5^\circ \times 2.5^\circ$  grid are resampled onto a polar stereographic grid for better visualization of the anomalies over the circumpolar Southern Ocean. Likewise, monthly sea surface temperature (SST) anomalies are resampled onto this same format. The mean monthly SST data on a  $1^\circ$  grid are the optimally interpolated fields of Reynolds and Smith (1994). Monthly anomalies are produced by first creating the monthly means, removing the monthly climatology, and then detrending the time series at each sample.

### b. Sea ice data

The 17 years of sea ice extent (SIE) and gridded sea ice concentration (SIC) derived from satellite passive microwave data are provided by the National Snow and Ice Data Center (NSIDC). Due to the dissimilarity of the Scanning Multichannel Microwave Radiometer (SMMR) and SSM/I sensors and mapping strategies, analyzed daily fields of SIE and SIC are available only after 1988. Prior to 1988, only 2-day SIE and SIC fields are available. The mean ice edge used here is defined as the mean latitudinal location of the SMMR and SSM/I ice edge over  $1^\circ$  sectors around the Antarctic continent.

Optimally interpolated fields of sea ice motion (SIM;

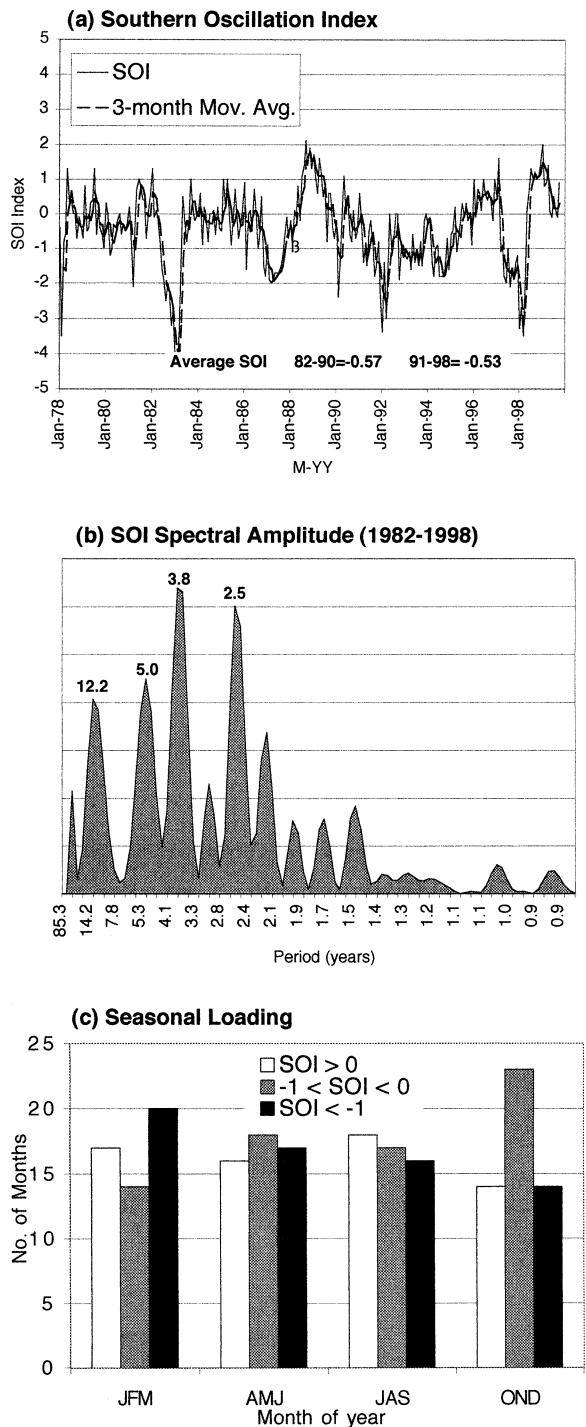


FIG. 1. The Southern Oscillation index. (a) The time series between 1978 and 1999. The dashed line shows the 3-month moving average of the time series. (b) Its wavenumber spectrum between 1982 and 1998. (c) Histogram comparing the seasonal loading (number of months) in each of the three phases of SOI ( $SOI > 0$ ,  $0 \geq SOI \geq -1$ ,  $SOI < -1$ ).

Kwok et al. 1998) are provided by the Jet Propulsion Laboratory (JPL) Remote Sensing Group. These analyzed motion fields are created by blending ice motion derived from two channels of satellite passive microwave data (37 and 85 GHz) and available ice displacements from drifting buoys. Only ice motion fields between the months of March and November are available since ice tracking results are unreliable during the summer and seasonal transitions. The monthly meridional (MIM) and zonal ice motion (ZIM) are on a 100-km polar stereographic grid.

The mean ice surface temperature (IST) fields used in this study were derived from AVHRR infrared data. The fields actually include sea surface temperature data as the retrievals extend beyond the ice edge. Because of persistent cloudiness in the coastal Antarctic and sub-Antarctic regions and the difficulty of discriminating clouds from snow-covered ice, a special cloud masking procedure was utilized, in addition to conventional techniques used over open ocean. Details of the retrieval procedure can be found in Comiso (2000). The uncertainties in the retrievals are estimated to be generally less than 3 K over ice-covered surfaces and less than 1 K over the open ocean. The data are mapped onto the polar stereographic format used for SSM/I data, with a grid size of 12.5 km.

Similar to the climate dataset, all monthly sea ice anomalies are produced by first creating the monthly means, removing the monthly climatology, and then detrending the time series at each sample location.

### 3. Data analysis

#### a. Correlation and composites fields

In this section, we examine the polar climate and sea ice anomalies associated with the SOI by correlation of the SOI time series with the climate anomalies and by forming composites of the climate and sea ice anomalies under the three phases of SOI defined above. At each sample location, the correlation coefficients between the time series of SLP, MW, ZW, SAT, and SST anomalies and the SOI time series are computed. The resulting correlation fields are shown in Fig. 2.

The statistical significance of the normalized cross-correlation coefficients depends on the length of the dataset and the smoothing applied. In the 17-yr dataset, there are 204 monthly data samples or there would be 202 degrees of freedom if the data samples were independent. However, both the smoothed SOI time series and the climate anomalies have nonzero autocorrelation, that is, they are serially correlated. The autocorrelation characteristics of the SOI time series can be clearly seen in Fig. 3. Thus, the confidence level of the observed correlations should be evaluated by procedures that can account for serial correlations. Here we select a non-parametric “random phase” method (Ebisuzaki 1997) to estimate the statistical significance of the correlation

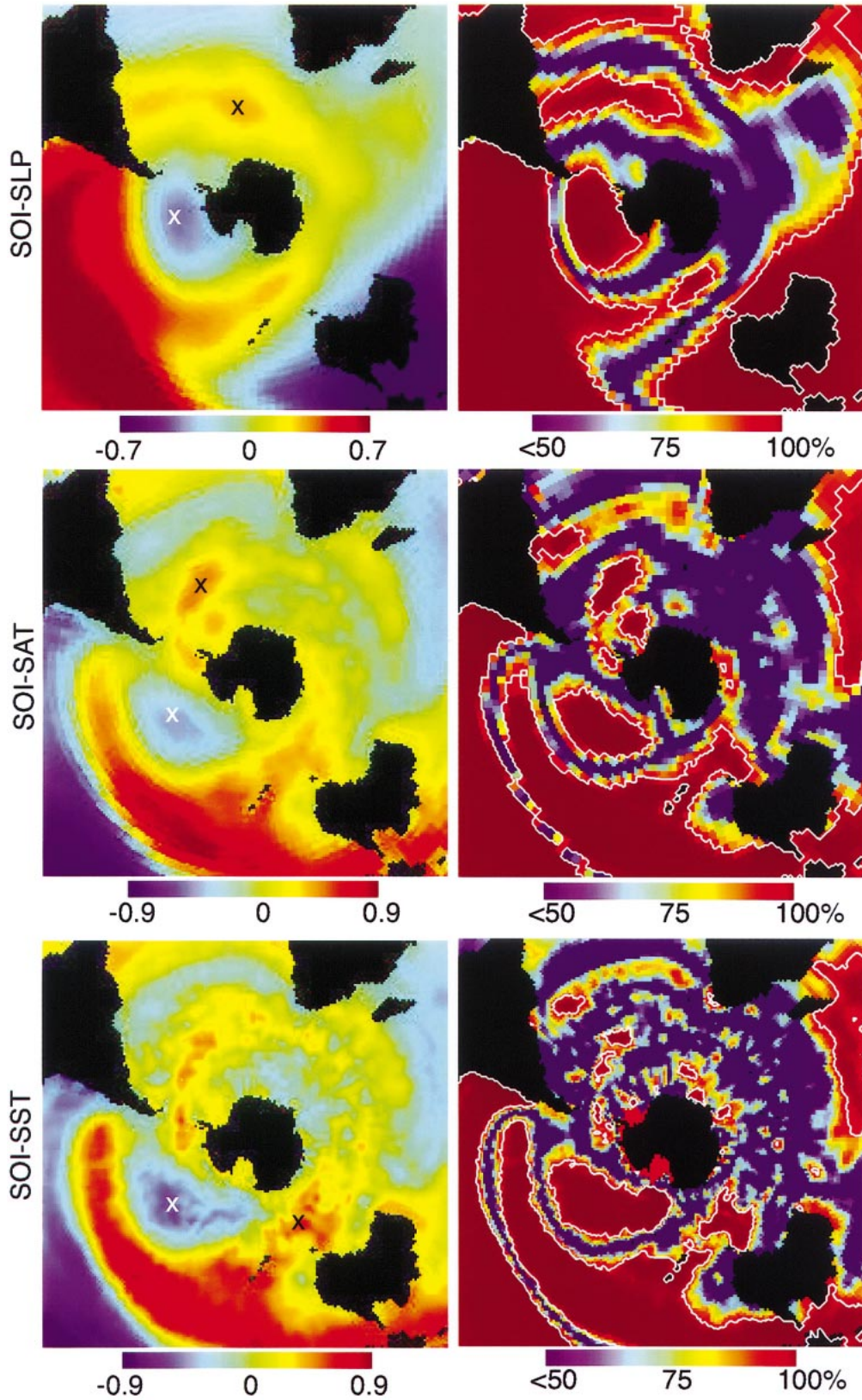


FIG. 2. Correlation of climate anomalies with SOI time series (1982–98) and the locations of the positive (black X) and negative (white X) extremes on the correlation maps. The confidence levels associated with the observed correlations are shown in a corresponding map. The white contours show the 95% confidence levels.

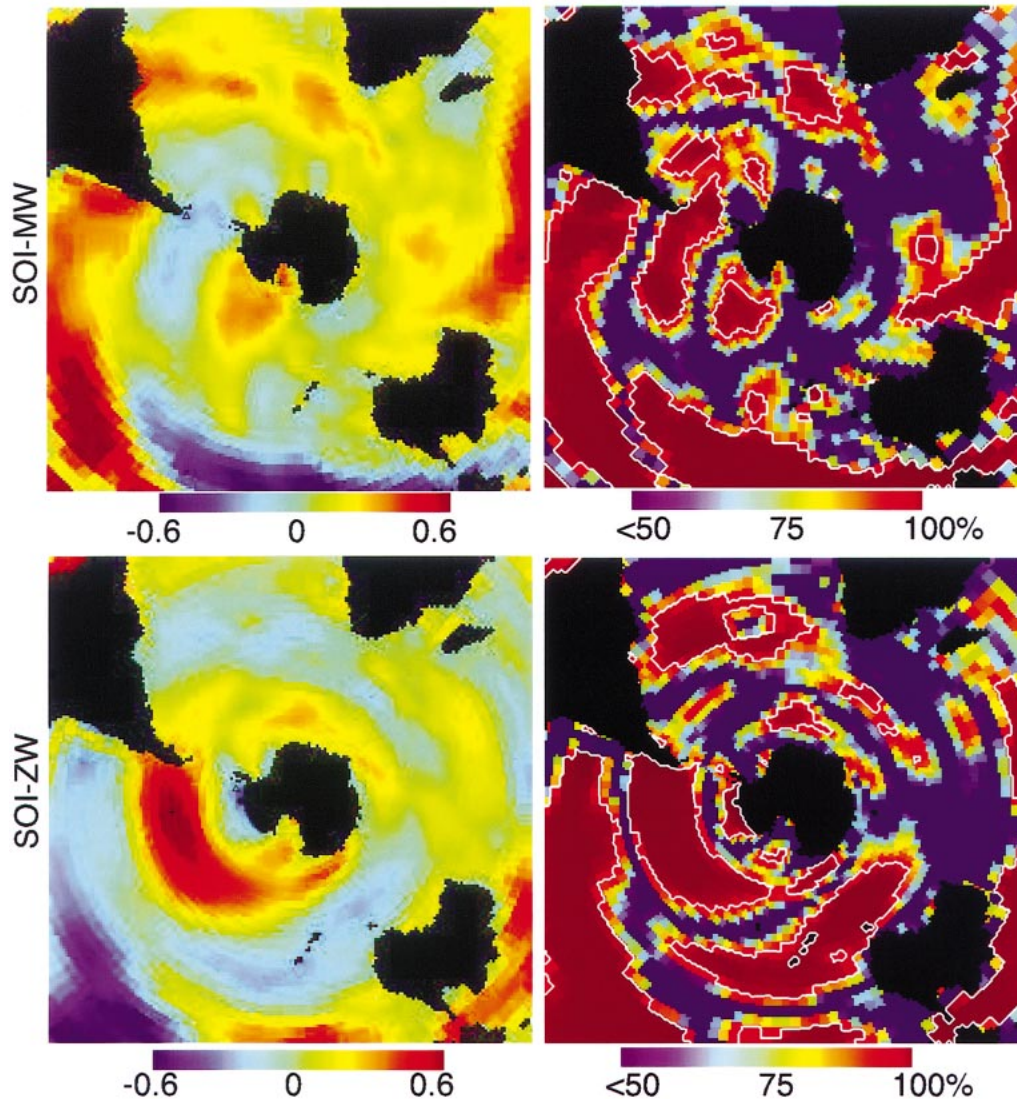


FIG. 2. (Continued)

coefficients. To estimate the confidence level at each spatial sample, this method involves creating a large number of different time series (in our case, 1000) with the same correlation characteristics as that of the SOI time series. Each realization is then correlated with the climate anomalies. If fewer than  $\alpha \times 100\%$  of the correlations from the random-phase series have magnitude greater than the observed correlation coefficient, then one can reject the null hypothesis,  $\rho = 0$ , at the  $\alpha$  significance level. Figure 2 shows the estimates of local confidence level associated with the correlation patterns obtained using this procedure.

Composite fields from three different phases of the SOI ( $\text{SOI} > 0$ ,  $0 \geq \text{SOI} \geq -1$ ,  $\text{SOI} < -1$ ) are constructed by averaging the monthly anomaly fields that fall within each of the three ranges of the SOI index. These composites allow us to examine the dominant

spatial pattern of the anomalies associated the oscillatory behavior of the SOI. Note that the phases that we select are not symmetric about zero. The rationale for this division is that over the 17 years between 1982 and 1998, the mean of the SOI index is nonzero and has a significant bias of  $-0.5$ . The division into these ranges gives us an approximately equal number of anomaly fields in each composite with 65, 72, and 67 monthly fields in the positive ( $\text{SOI}^+$ ), neutral ( $\text{SOI}^0$ ), and negative ( $\text{SOI}^-$ ) phases, respectively. Within each phase, the seasonal loading of the monthly fields is shown in the histogram of Fig. 1. The histogram shows that there are more months from the austral spring in the neutral phase, while there are more months from the austral summer in the negative phase. However, we do not feel that there is a large enough sample population for one to conclude that the composite fields are representative

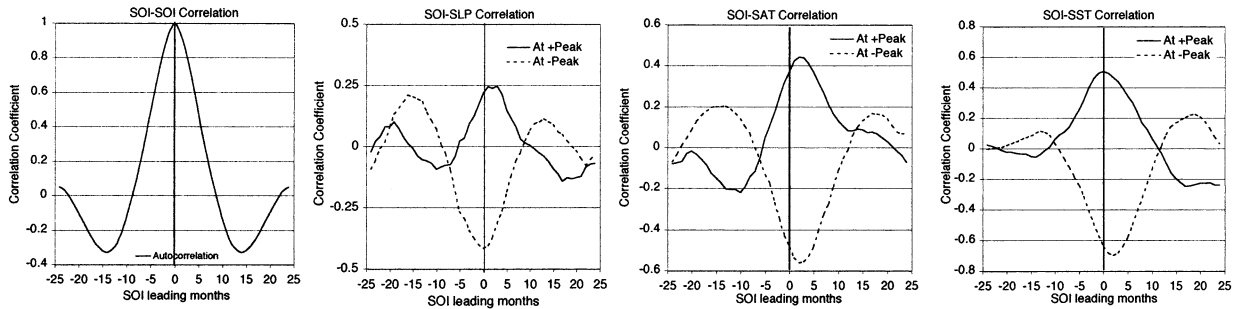


FIG. 3. Lag-correlation plots of the SLP, SAT, and SST anomalies with the SOI time series at the positive and negative correlation extremes (positive indicates SOI leads). The autocorrelation of the SOI time series is also shown.

of a particular austral season. In the remainder of this section, we describe the patterns observed in the correlation maps and the composite fields, and comment on the stability of the anomaly fields.

### b. Polar climate anomalies

The correlation amplitudes show distinct centers of action in the correlation maps (positive and negative extremes in the correlation coefficient) of the polar climate anomalies and SOI (Fig. 2). The lag-correlation plots between the time series of climate anomalies and SOI at the locations of strongest positive and negative correlation south of  $50^{\circ}\text{S}$  are shown in Fig. 3. We examine only the correlation extremes in the polar latitudes as our interests are in the association of the anomalies with the SO pattern. Figure 4 shows the composite fields of climate anomalies under the three phases ( $\text{SOI}^+$ ,  $\text{SOI}^0$ ,  $\text{SOI}^-$ ) of SOI as well as the differences between the  $\text{SOI}^+$  and  $\text{SOI}^-$  composites. This difference of the composites accentuates the contrast between the two extreme phases, especially when the anomalies are of opposite polarities.

#### 1) SEA LEVEL PRESSURE AND WINDS

Over the entire domain, the SLP–SOI correlation map is dominated by the region of strong negative correlation (Fig. 2) in the eastern Indian Ocean northwest of Australia and the region of strong positive correlation in the subtropical eastern Pacific near Tahiti. This is the expected SLP anomaly pattern associated with the Southern Oscillation. Poleward of  $50^{\circ}\text{S}$ , there are three centers of action in the following regions: a sector of negative correlation between the Ross Sea and the Antarctic Peninsula (peak  $\sim -0.42$ ) flanked by two narrower sectors of weaker positive correlation east of the Weddell Sea and west of the Ross Sea. Negative correlation indicates a time series of SLP anomalies that is out of phase with the SOI. In an analysis of the teleconnections in the Southern Hemisphere, Mo and White (1985) also found that zonally averaged pressure anomalies at sea level display an out-of-phase relation between low and high latitudes, and in midlatitudes are negatively correlated

with anomalies in the subtropics and polar regions. They suggested a strong resemblance to the oscillatory behavior associated with the SO as is seen here.

Between  $50^{\circ}$  and  $60^{\circ}\text{S}$ , the SLP–SOI correlation field exhibits a wavenumber-2 pattern around the circumpolar Southern Ocean. As seen in the lag-correlation plots (Fig. 3) the spatial peaks are also distinct in time and the broad correlation structure shows similarity to the autocorrelation signature of the large-scale coherent SOI signal (Fig. 3). There is no observable lag between the SLP anomalies and SOI at the location of the negative peak (centered between the Amundsen and Bellingshausen Seas). An approximate 2-month lag, with the SLP anomalies lagging the SOI, is evident at the location of the positive peak (centered along the prime meridian).

In the SOI–SLP composite (Fig. 4), the typical ENSO pattern of positive SLP anomalies over northwest Australia and negative SLP anomalies over the subtropical eastern Pacific can be seen. The SO, indicated by large negative SOI indices, has a signature that clearly extends to the mid- and polar latitudes of the Southern Hemisphere. South of  $50^{\circ}\text{S}$ , two distinct spatial patterns of SLP are associated with the two extreme phases of SOI. In the  $\text{SOI}^+$  SLP composite, a sector of negative SLP anomaly is located off the Antarctic coast in the Amundsen and Bellingshausen Seas. An almost exact anomaly pattern of opposite polarity can be found in the  $\text{SOI}^-$  SLP composite.

The above-normal SLP south of  $50^{\circ}\text{S}$  associated with ENSO episodes ( $\text{SOI}^-$ ) was reported by Karoly (1989), but the strength of the pattern and the opposite behavior during  $\text{SOI}^+$  are shown for the first time with some spatial detail in this study. It is interesting to note that the SLP anomalies in the sector between  $170^{\circ}$  and  $60^{\circ}\text{W}$  are more spatially localized and more extreme than SLP anomalies at the two centers of action of the SO in the tropical latitudes. Within the domain shown in Fig. 4, the dominant SLP anomaly can be found centered in the Amundsen and Bellingshausen Seas region. The strong correlation of the region with ENSO episodes indicate that the climate anomalies in the region (Jacobs and Comiso 1997; King and Harangozo 1998) are as-

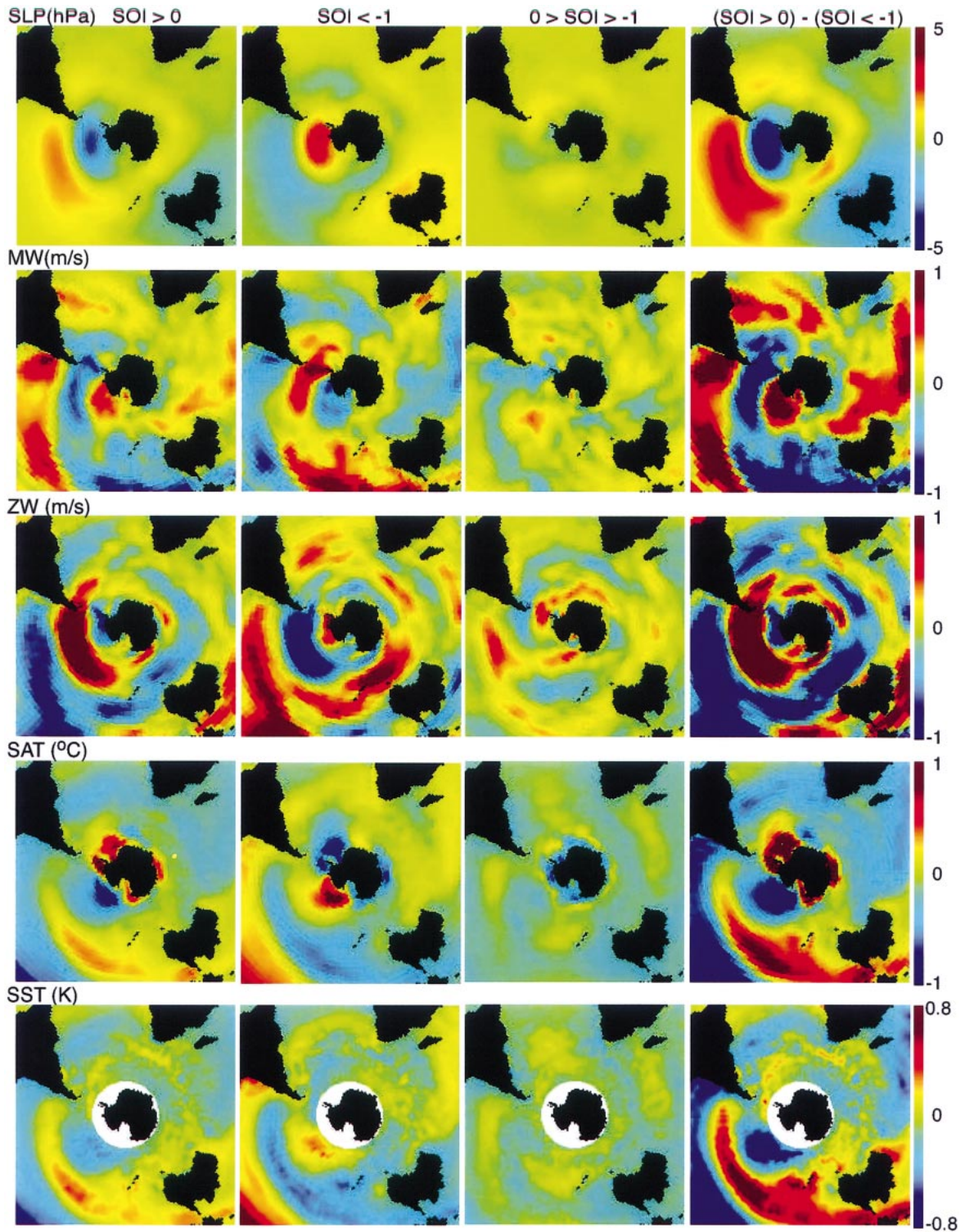


FIG. 4. Composites of climate anomalies (1982–98) during three phases of SOI ( $SOI > 0$ ,  $0 \geq SOI \geq -1$ ,  $SOI < -1$ ) and the difference between the two extremes ( $SOI > 0$  and  $SOI < -1$ ).

sociated with occurrences of ENSO. Between the two extremes ( $SOI^0$ ), the anomalies are smaller. These composite patterns are persistent with varying intensity throughout the year as observed in the December–January–February (DJF), March–April–May (MAM), June–July–August (JJA), and September–October–November (SON) composites (not shown here). The most extreme pattern can be seen in the SON fields.

The SLP anomalies alter the meridional and zonal wind anomalies and in turn affect the SIM and SIE. The  $SOI$ –MW correlation field (Fig. 2) shows a sector of positive correlation between the Ross Sea ( $170^\circ E$ ) and east Amundsen Sea ( $100^\circ W$ ) and a sector of negative correlation between the Bellingshausen Sea and the Antarctic Peninsula. The ZW– $SOI$  correlation map shows a sector of positive correlation between  $50^\circ$  and  $60^\circ S$  between the Ross Sea and north of the Antarctic Peninsula. A narrow band of negative correlation, within the sea ice cover, can be found south of  $60^\circ S$  along the Antarctic coast in the Amundsen and Bellingshausen sectors. These patterns are consistent with the anomalous circulation patterns due to the SLP anomalies discussed above.

Similar to the SLP composites, the MW and ZW anomalies have distinct spatial patterns and opposite polarities at the  $SOI$  extremes (Fig. 4). Here, a sector of positive MW anomalies covering the Ross Sea and the Amundsen Sea can be found in the  $SOI^+$  composite. The negative MW anomalies straddle the Antarctic Peninsula and cover a sector containing part of the Bellingshausen Sea and Weddell Sea. Opposite patterns are found during  $SOI^-$ . South of  $60^\circ S$  in the  $SOI^-$  ZW composites, positive zonal wind anomalies can be found in the Amundsen and Bellingshausen Seas, and parts of the Weddell Sea. North of  $60^\circ S$ , there is a large sector with negative ZW anomalies.

## 2) SURFACE AIR TEMPERATURE

Three distinct  $SOI$ –SAT correlation bands can be seen in the Pacific Ocean sector (Fig. 2): a band of negative correlation in the equatorial Pacific, a band of positive correlation between  $30^\circ$  and  $45^\circ S$ , and a band of negative correlation south of  $50^\circ S$ . Negative correlation indicates warmer SATs associated with negative excursions of the  $SOI$ . South of  $50^\circ S$ , there are two centers of action: a sector of negative correlation (negative peak  $\sim -0.59$ ) centered between the Ross Sea and the western Bellingshausen Sea and a sector of positive correlation (peak  $\sim 0.44$ ) centered between the Bellingshausen and the Weddell Seas. Both the positive and negative peaks lag the  $SOI$  by approximately 2–3 months.

The three bands in the  $SOI^-$  SAT composites (Fig. 4) are associated with warm/cold/warm anomalies in the tropical and subtropical Pacific during ENSO episodes. Similarly, the  $SOI^+$  and  $SOI^-$  SAT composites present two distinct and opposite patterns of SAT anomalies. South of  $50^\circ S$ , the  $SOI^+$  SAT composite shows a sector

of below-normal SAT in the region between the Ross Sea and the Amundsen Sea and a sector of warmer SAT covering the Bellingshausen Sea and Weddell Sea. Again, an approximate opposite pattern is seen during  $SOI^-$ . These patterns are robust in the seasonal fields, with the SON field showing the largest extremes. A wavenumber-2 pattern, within the sea ice zone, encircling the pole is evident.

## 3) SEA SURFACE TEMPERATURE

The SAT and SST correlation maps (Fig. 2) are similar, three correlation bands can be seen in the Pacific Ocean: negative correlation covers one band in the equatorial Pacific, a midlatitude band of positive correlation between  $30^\circ$  and  $45^\circ S$ , and a band south of  $50^\circ S$ . Warmer SSTs are associated with negative excursions of the  $SOI$ . South of  $50^\circ S$  and off the sea ice zone, there are two centers of action: a sector of strong negative correlation (peak  $\sim -0.7$ ) centered between the Ross and western Bellingshausen Seas and a sector of positive correlation (peak  $\sim 0.5$ ) south of Tasmania. Distinct peaks can be seen in the lag-correlation plots. The negative correlation peak lags the  $SOI$  by 2–3 months.

Similar to the SAT, three bands in the  $SOI^-$  SST composites are associated with warm/cold/warm sea surface temperature anomalies in the Pacific during ENSO episodes. South of  $50^\circ S$ , two distinct and opposite patterns of SST anomalies are associated in the  $SOI^+$  and  $SOI^-$ . A sector of above SST can be seen in the region between the Ross and western Bellingshausen Seas in the  $SOI^-$  SST composite. This is associated with the large positive SST anomalies in the central equatorial Pacific Ocean. A similar pattern of opposite polarity is in the  $SOI^+$ . A wavenumber-2 pattern is seen in both the correlation and composite fields.

## 4) SUMMARY OF POLAR CLIMATE ANOMALIES

As revealed in the correlation maps and anomaly composites, the covarying climate anomalies in the Amundsen, Bellingshausen, and Weddell Seas show the strongest link to the  $SOI$ . The spatial structure of the connections between the anomalies and  $SOI$  are localized and well defined. Within these sectors, positive (negative) phases of the  $SOI$  are generally associated with lower (higher) sea level pressure, cooler (warmer) surface air temperature, and cooler (warmer) sea surface temperature in these sectors. The SLP, SAT, and SST correlation fields and composites show wavenumber-2 patterns that are suggestive of the anomalies at  $56^\circ S$  reported in White and Peterson (1996) although the peaks in these anomalies are found south of  $60^\circ S$ . The composite fields depict the mean anomalies over the three ranges of  $SOI$  defined here. In all the composites, it is remarkable that the anomaly patterns associated with the two extremes are distinct and are of opposite polarities. The broad correlation structure seen in the

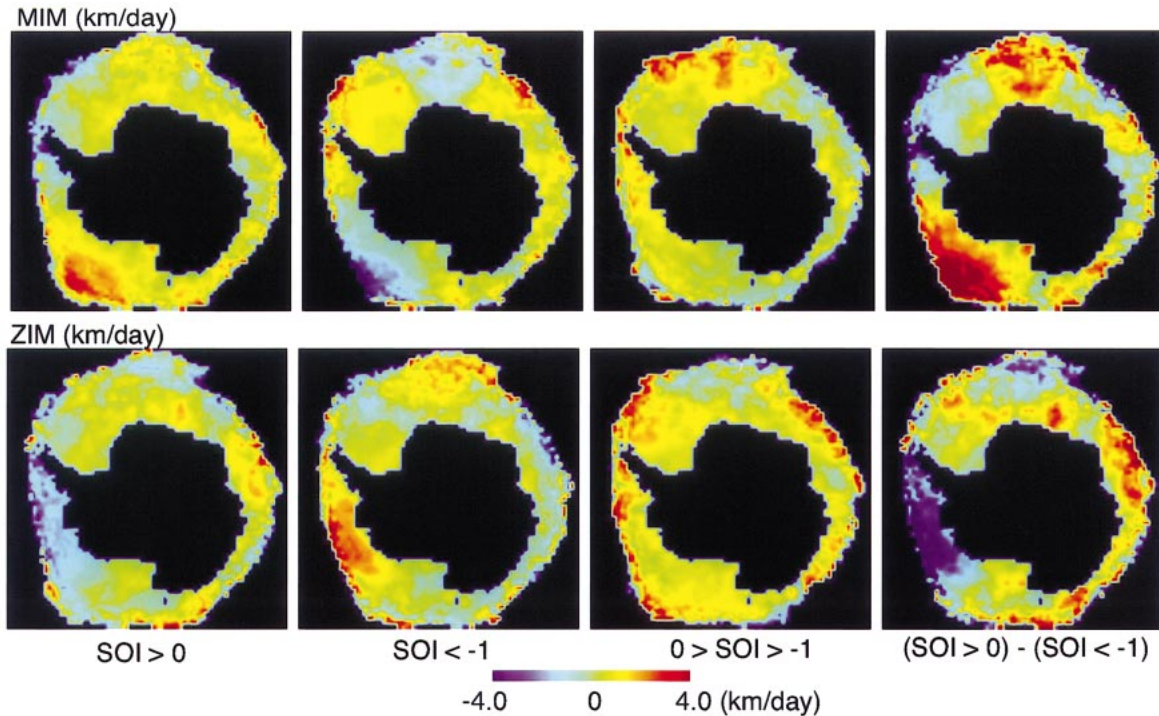


FIG. 5. Composites of winter ice motion anomalies (Mar–Nov, 1982–98) during three phases of SOI ( $SOI > 0$ ,  $0 \geq SOI \geq -1$ ,  $SOI < -1$ ) and the difference between the two extremes ( $SOI > 0$  and  $SOI < -1$ ).

lag-correlation plots shows similarity to the autocorrelation signature of the large-scale coherent SOI signal (Fig. 3). The lag correlations at the correlation peaks are interesting in that in all cases the SOI is either contemporaneous or leads the SLP, SAT, and SST fields. The underlying mechanisms are, however, not well understood.

### c. Antarctic sea ice anomalies

#### 1) SEA ICE MOTION

The three composites of ice motion are shown in Fig. 5. Through wind forcing, the SLP anomalies over the Antarctic ice cover are coupled to the anomaly patterns of sea ice circulation. Anomalies in ice motion affect ice transport and ice extent. The pattern of winter (March–November) meridional (MIM) and zonal (ZIM) ice motion anomalies are well correlated with the MW and ZW anomalies. This is not unexpected since away from coastal boundaries, geostrophic wind explains more than 70% of the variance of daily ice motion in both winter and summer. During  $SOI^+$ , a broad sector of positive MIM anomalies covers the Ross and Amundsen Sea ice covers. The negative MIM anomalies are located in the Bellingshausen and Weddell Seas. The  $SOI^-$  MIM composite shows anomalies of the opposite polarity compared to the  $SOI^+$  MIM composite. In the  $SOI^0$  composite, a sector of positive anomaly can be found covering the ice cover between  $20^\circ W$  and  $20^\circ E$ .

Similarly, ZIM anomalies are coupled to the ZW anomalies. Negative (positive) ZIM anomalies in the  $SOI^+$  ( $SOI^-$ ) composites cover the Amundsen and Bellingshausen Seas. Under  $SOI^-$  conditions, a sector of positive ZIM anomalies can be found east of the Weddell Sea centered around the prime meridian. Extremes in ZIM anomalies can be found during the austral winter over the months of JJA and SON (not shown here).

#### 2) ICE SURFACE TEMPERATURE

Figure 6 shows the SOI–IST correlation pattern and the composites of IST anomalies, derived from AVHRR data for the 17-yr period. As mentioned above, the IST fields actually include sea surface temperature data as the retrievals extend beyond the ice edge. Within the sea ice cover, there is a sector of positive correlation between the Bellingshausen and Weddell Seas. In contrast, the region of negative correlation is actually situated on the sea surface (Amundsen and Ross Seas) off the ice cover. A distinct wavenumber-2 pattern can be seen in the composites. Alternating positive and negative IST anomalies can be seen to cover two zones of the ice cover during  $SOI^+$  with positive anomalies covering the following areas: the Bellingshausen and Weddell Seas, between  $80^\circ$  and  $10^\circ W$ , and between  $100^\circ$  and  $120^\circ E$ . Similar but opposite anomaly patterns are observed during  $SOI^-$ . The significance of IST anomalies over the ice cover is that they affect the radiation balance

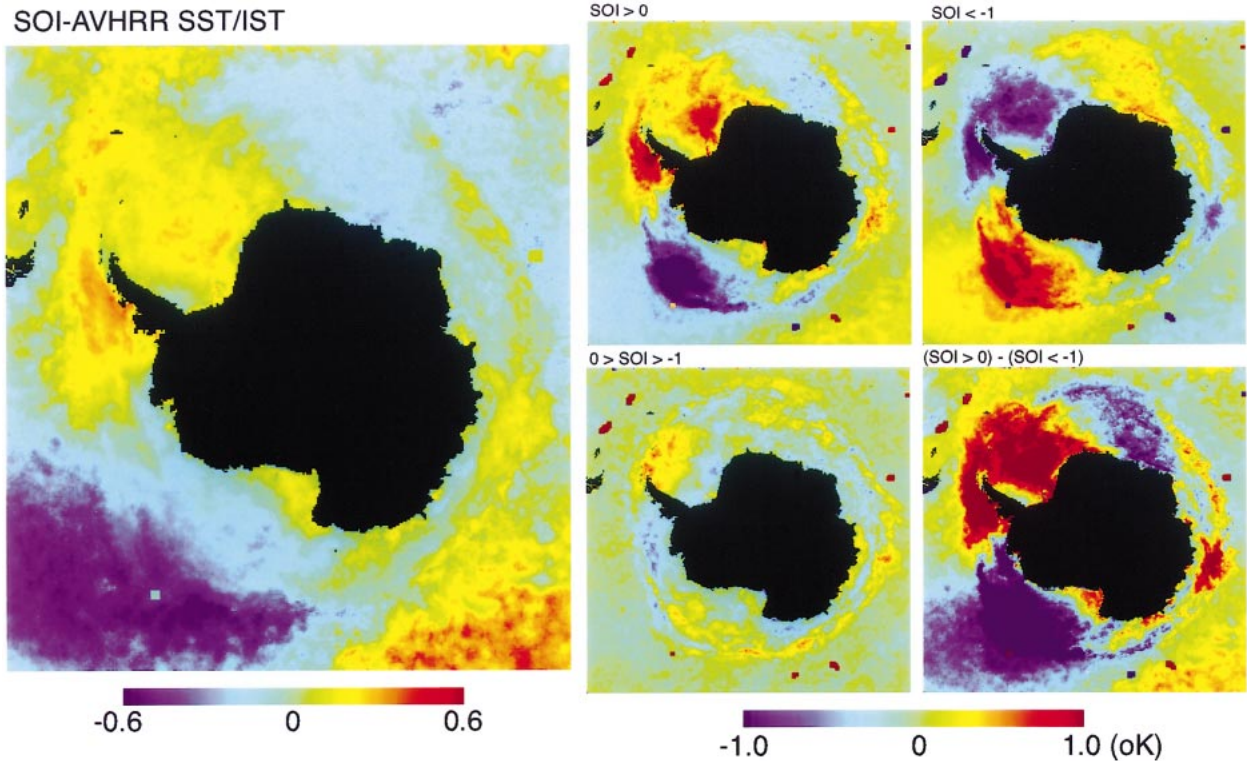


FIG. 6. (a) Correlation of the AVHRR-derived IST and SST with the SOI. (b) Composites of surface temperature anomalies (1982–98) during the three phases of SOI ( $\text{SOI} > 0$ ,  $0 \geq \text{SOI} \geq -1$ ,  $\text{SOI} < -1$ ) and the difference between the two extremes ( $\text{SOI} > 0$  and  $\text{SOI} < -1$ ).

at the surface and thus the rate of ice growth and brine rejection into the ocean.

These IST anomalies are also associated and resemble those of the SST near the ice edge (Fig. 2). This is especially evident with the negative (positive) SST anomalies in the Amundsen and Ross Seas during  $\text{SOI}^+$  ( $\text{SOI}^-$ ).

### 3) SEA ICE EXTENT AND CONCENTRATION

The composites of SIE and SIC anomalies associated with the three phases of SOI are shown in Fig. 7. In the  $\text{SOI}^+$  ( $\text{SOI}^-$ ) composites, positive (negative) anomalies of the SIE are located between  $180^\circ$  and  $130^\circ\text{W}$  in the Ross and Amundsen Seas, negative (positive) anomalies can be found between  $100^\circ\text{W}$  and  $10^\circ\text{E}$  in Bellingshausen and Weddell Seas, and, smaller positive (negative) anomalies are found in the sector between  $10^\circ$  and  $50^\circ\text{E}$ . The anomalies in the other sectors of the Antarctic are insignificant during all three phases of the SOI. It is interesting to note that the SIE anomalies in the eastern Bellingshausen Sea are out of phase with those in the Amundsen Sea even though they are geographically contiguous. This out-of-phase relationship between the Bellingshausen and Amundsen sea ice edge can also be seen in the circumpolar lag correlation between the SOI and SIE anomalies (Fig. 8). The SOI lags the SIE anomalies in the Bellingshausen and eastern Weddell Seas by

2–3 months while the SOI leads the SIE in the Amundsen and Ross Seas. At zero lag, a wavenumber-2 pattern is also evident in the plot. The diagonal bands in Fig. 8 hint of eastward propagating SIE anomalies (associated with the SOI) between  $180^\circ$  and  $360^\circ\text{E}$  with a circumpolar period of about 7–8 years (ACW-like signal) but this propagating pattern is not evident over the east Antarctica sea ice cover.

The largest SIC anomalies are located off the Antarctic coast near the ice edge. Also, the SIC anomalies are collocated within the same sectors as those of the SIE anomalies. Figures 7 and 8 show that positive anomalies of the SIE are coupled with positive SIC anomalies while negative SIE anomalies are associated with negative SIC anomalies. This association of SIE and SIC anomalies of the same polarity would seem counterintuitive if SIE anomalies are explained only by wind and ice motion, as divergence (convergence) would lead to negative (positive) ice concentration anomalies. The positive (negative) anomalies in the ice edge especially in the Ross and Amundsen Seas are indeed associated with positive (negative) anomalies in the meridional winds and ice motion (Fig. 4). However, these are also associated with negative (positive) anomalies in the SST and IST (Figs. 4 and 6) that favor (discourage) ice growth. As a result, the positive (negative) MW anomalies and ice motion anomalies favor expansion (retreat) in the ice edge, while cooler (warmer) SST and IST also

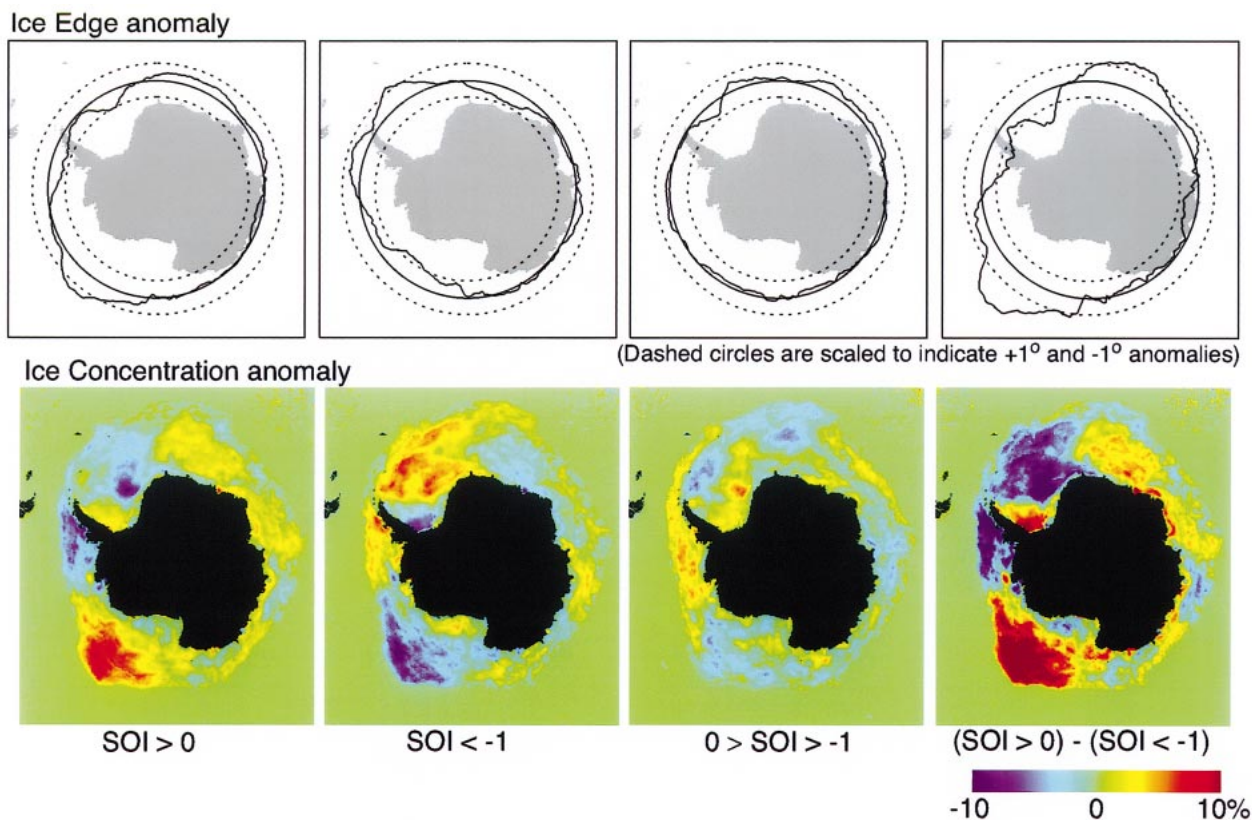


FIG. 7. Composites of ice edge/concentration anomalies (1982–98) during three phases of SOI (SOI > 0,  $0 \geq \text{SOI} \geq -1$ , SOI < -1) and the difference between the two extremes (SOI > 0 and SOI < -1). The anomalies are scaled to emphasize the spatial pattern. Dashed circles indicate  $\pm 1^\circ$  anomalies in the ice edge location.

allow ice growth (melt) in place and thus the relative persistence of the ice cover or higher (lower) ice concentration. This suggests that the ice edge and ice concentration anomalies are sustained by ice kinematics as well as thermodynamics with significant roles played by the anomalies in the SST and SAT.

The Bellingshausen, Amundsen, and Ross Sea sectors have the most significant connection to the Southern Oscillation. Spatially distinct anomaly patterns in the climate as well as sea ice variables are apparent in the vicinity of this region. The teleconnection is clearly indicated in the plots of the ice edge trend and the monthly time series of sea ice extent and ice area anomalies in Fig. 9. In both ice extent and ice area plots, anomalously low values occurred in 1983, 1987, 1992, and 1998. These are the same years that were pointed out earlier (see Fig. 1) as ENSO years. Similar anomalies for these same years did not occur in the sea ice variables in other Antarctic regions. The trend in the ice edge (Fig. 9) resembles the anomalies that are characteristic during the negative phase, that is, ice edge retreat in the Bellingshausen, Amundsen, and Ross Seas (Fig. 7). Even though there is no significant trend in the SOI over the 17 years, this is the only region with an observable negative trend in ice cover over the 20 years. The trend

is possibly weighted by the four significant ENSO episodes. The satellite time series in fact shows that the climatological behavior of the ice cover in the Bellingshausen–Amundsen Sea region is unique in its relation to the Southern Oscillation. A question of interest is whether the climate of the region is different from other regions because of its unique connection to the Southern Oscillation.

#### d. Stability of composite fields

The composite fields described in the previous section have been prepared over a relatively short 17-yr period. An assessment of the stability of these composites has been carried out in two ways. First, the climate data are divided up into two 8-yr records to determine whether the anomalies are spatially stable and give comparable magnitude of anomalies in the same regions. In all cases, the differences are minor and do not change the conclusions drawn here. Second, we produced seasonal composites (DJF, MAM, JJA, SON) to examine the stability of the anomalies constructed in this manner. While the locations of the anomalies remain relatively stable in the seasonal fields, the magnitudes do vary. The seasonal dependence of the magnitude of the anomalies,

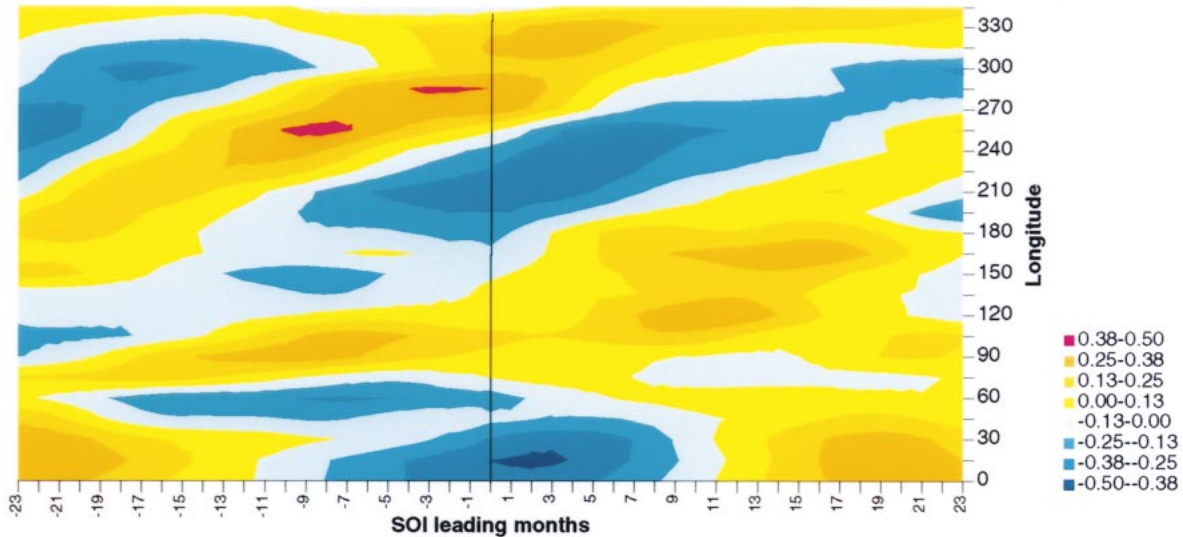


FIG. 8. Lag correlations between sea ice edge anomalies and SOI (1982–98) (positive indicates that SOI leads).

even though not shown here, was discussed in the previous section.

#### 4. Discussion

In this section, we discuss in more detail the covarying climate and sea ice anomalies in the context of the results from previous studies. Clearly, the correlation maps and the anomaly composites show coherent links between the Southern Ocean climate and sea ice processes and the Southern Oscillation. The question is whether our results describing the associations between the SOI and sea ice anomalies are consistent with observations of sea ice anomalies from previous studies.

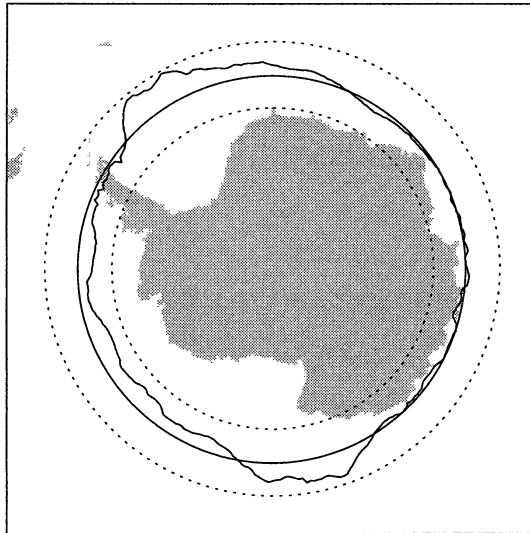
A number of studies have focused on the record of the Southern Ocean sea ice extent/edge and its relationship to climate variables and indices. Here, these observed trends and anomalies are discussed within the context of our results that describe the large-scale sea ice anomalies associated with the three phases of SOI over the 17-yr period between 1982 and 1998.

Jacobs and Comiso (1993) attributed the record decrease in the sea ice extent in the Bellingshausen Sea from mid-1998 to early 1991 to more southerly surface winds and historic high surface air temperatures along the west coast of the Antarctic Peninsula in 1989. They also reported that this retreat was preceded by a higher than normal ice cover in 1986–87. An updated plot (1978–99) of the monthly ice extent and ice area anomalies in the Bellingshausen–Amundsen Sea sector is shown in Fig. 9. Our composites (in Figs. 2–7) show a large-scale view of the associated climate and sea ice anomalies that are consistent with their observations. The years between 1986 and early 1991 bracket a period with an ENSO episode (SOI<sup>-</sup>) in 1987 followed by a La Niña event (SOI<sup>+</sup>) in 1989. Over this period, a pos-

itive anomaly followed by a negative anomaly in the Bellingshausen Sea ice cover is clearly seen in the SOI<sup>-</sup> (SOI<sup>+</sup>) SIE anomaly composites. The positive (negative) anomaly in ice extent is associated with cooler (warmer) SATs and ISTs, and positive (negative) meridional winds and ice motion anomalies due to the positive (negative) SLP anomalies in the Amundsen and Bellingshausen Seas. An above-normal ice cover during SOI<sup>-</sup> was followed by a below-normal ice cover during SOI<sup>+</sup>. Thus, this contrast in the ice extent over the two phases of SO accentuates the observed retreat of the ice cover.

In another study using an ice extent dataset spanning 1973–94, Jacobs and Comiso (1997) reported a decline in the sea ice extent in the Amundsen and Bellingshausen Seas in two decades following 1973. The northern ice edge retreated by approximately 1° of latitude in all seasons from 1973–79 to 1987–93 (also see Fig. 9). They suggest that the mean and extreme ice extents are linked to large-scale circulation changes in the South Pacific. Over the 21-yr period from 1973 to 1993, the linear trend of the SOI shows a significant decrease of  $-1.6$  (standard deviation = 1.2) from 0.4 to  $-1.2$ . In the progression from SOI<sup>+</sup> to SOI<sup>-</sup> conditions over the period, our composites (Figs. 2–7) indicate warmer SSTs, SATs, ISTs, and more northerly wind conditions in a large part of the Amundsen and western Bellingshausen Seas. The trend is also toward negative SIE anomalies in the Amundsen Sea. The slight positive SIE anomalies in the Bellingshausen Sea were not mentioned in the study since the SIE of the two seas were not treated separately. In any case, the area of the Amundsen Sea ice cover dominates the pattern. Hence, our composite fields can be used to explain the general conditions of the ice cover associated with the Southern Oscillation.

Scaled Linear Trend in Ice Edge (1982-1998)



(Dashed circles are scaled to indicate +0.1°/yr and -1°/yr trends)

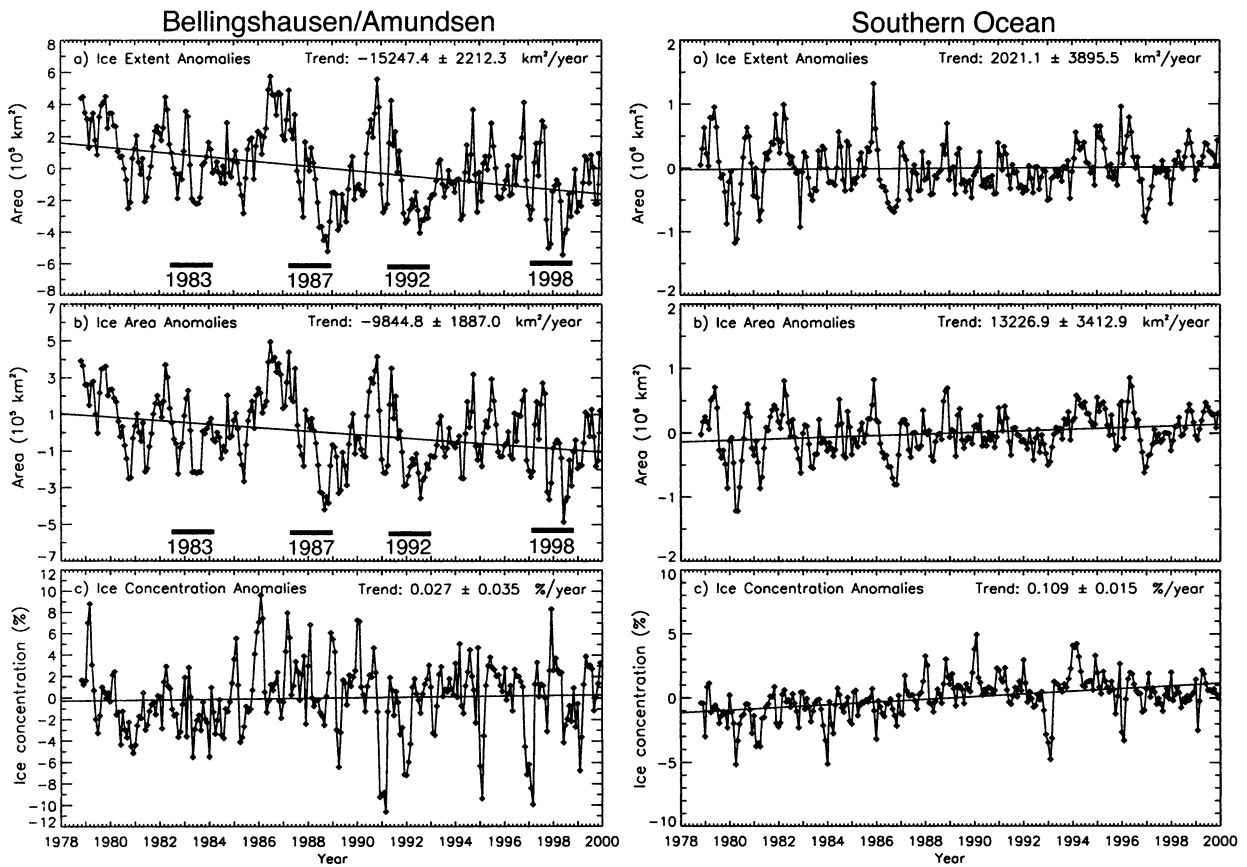


FIG. 9. (a) The 17-yr (1982–98) trend in the ice edge. (The trends are scaled to emphasize the spatial pattern. Dashed circles indicate ±0.1° yr<sup>-1</sup> trends in the ice edge location.) (b) Comparison of the anomalies and the trends in sea ice extent, area, and concentration between the Amundsen and Bellingshausen Seas and the entire Antarctic Sea ice cover from 1978 to 1999. The trends have not been removed in these plots.

Simmonds and Jacka (1995) explored links between Antarctic sea ice extent and the SOI using a dataset spanning 1973–92. They found correlations in the southwest Indian Ocean sector, the southwest and southeast Pacific Ocean sector, and a sector to the west of the Ross Sea. Their exploratory procedure was to calculate the correlation of the sea ice extent, averaged over various longitudinal domains in each calendar month, with the smoothed SOI values in all months in the same year and also the previous year and subsequent years. Their approach has the advantage of being able to localize the seasonal correlations with SOI, but their results are limited by a rather short data span of 20 points (or 18 degrees of freedom). Here, we compute the correlations based on the entire time series of SOI and ice edge anomaly. In this case the results are slightly different, they did not report the significant correlations in the Amundsen Sea, Bellingshausen Sea, and Weddell Gyre found here that are also reported by Yuan and Martinson (2000).

Ledley and Huang (1997) examined the sea ice concentration between 1982 and 1994 (which covered three ENSO episodes) and found that there is a statistically significant relationship between Ross Sea SST and sea ice concentration, with warm (cold) temperature anomalies corresponding to decreases (increases) in sea ice concentration. They report that the Ross Sea SST anomalies are in turn positively correlated with the Niño-3 SST. Their maximum correlation ( $r = 0.72$ ) occurs with a lag of 3 months with the Ross Sea SST lagging the ENSO signal. Similarly, south of 50°S, we find a comparable negative peak in the correlation between the SOI and SST anomalies ( $r = -0.7$ ) located in the eastern Ross Sea (Fig. 2) with the SST anomalies lagging the SOI by about 2–3 months. We also found negative (positive) anomalies in ice concentration (Fig. 7), associated with the warmer (cooler) SST and IST.

In an analysis of the length of sea ice season between 1988 and 1994, Parkinson (1998) captured one cycle of the SOI. A positive peak in the SOI in 1989 was followed by an ENSO episode in 1992. Based on linear trends over the seven years of data, the results show that the ice seasons have shortened in the eastern Ross Sea, Amundsen Sea, far western Weddell Sea, and non-coastal far eastern Weddell Sea and the coastal regions of east Antarctica, and have lengthened in the western Ross Sea, Bellingshausen Sea, and central Weddell Sea, and the 80°–135°E sector off the coast of east Antarctica. With our results, the difference in the anomalies in the ice extent associated with the SOI<sup>-</sup> and SOI<sup>+</sup> extremes (Fig. 7) provide an indication of the trend over the seven years even though the ice extent anomaly is only a proxy indicator of the length of the ice season. We expect the largest variability in length of seasons to be near the ice edge. Over the seven years, our composites indicate that there should be a negative trend in the ice extent over the Ross Sea, the Amundsen Sea, eastern Weddell Sea, and an increase in the Bellingshausen and central Wed-

dell Seas. The anomalies over the east Antarctic sector are not as clear. In general, there are broad agreements between our analyses and with the observed trends especially in the Pacific and Atlantic sectors. Again, these are associated with the covarying fields of climate and sea ice anomalies linked to the SOI.

In a recent work, Yuan and Martinson (2000) summarized the possible relationship between the Antarctic sea ice extent (1978–96) and global climate variability. They also show that the SIE in the Amundsen Sea, Bellingshausen Sea, and Weddell Gyre of the Antarctic polar ocean sectors show the strongest link to extrapolar climate. Our results are in agreement with their observations regarding the relationship between the ENSO signal and the ice extent.

## 5. Conclusions

The spatial signature of the climate and sea ice anomalies in the Southern Ocean associated with the Southern Oscillation are revealed in the correlation patterns and the composite fields. The correlation maps and lag-correlation plots show features of the spatial and temporal relationships between these anomalies and the index of Southern Oscillation, while the composite maps show the dominant spatial signature of the anomalies during the three phases of SOI. On a large scale, these anomalies are organized in coherent patterns and assume opposite polarities during the two extremes of SOI. Also, these anomalies covary with the Southern Oscillation and oscillate at approximately the same frequency. Association with ENSO-related activities in the equatorial Pacific is clearly indicated.

Overall, the climate anomalies in the Amundsen, Bellingshausen, and Weddell Sea sectors of the Antarctic polar ocean show the strongest link to the Southern Oscillation. Within these sectors, the climate anomalies show the highest correlation with the SOI and the composite patterns show the most intense and localized climate and sea ice anomalies associated with the extremes of SOI. Positive (negative) phases of the SOI are generally associated with lower (higher) sea level pressure, cooler (warmer) surface air temperature, and cooler (warmer) sea surface temperature in these sectors. Outside these sectors, the anomalies are not as distinct.

Linkages between the SOI, the climate anomalies, and the sea ice extent, concentration, motion, and ice surface temperature are also evident. The sea ice cover anomalies are located within the same sectors as those with the dominant climate anomalies. During the positive (negative) phase of SOI, positive (negative) anomalies of the SIE are located between 180° and 130°W in the Ross and Amundsen Seas, negative (positive) anomalies can be found between 100°W and 10°E in Bellingshausen and Weddell Seas, and, smaller positive (negative) anomalies are found in the sector between 10° and 50°E.

The physical mechanisms by which these polar processes are linked to the Southern Oscillation are com-

plex and beyond the scope of this study. However, the identified relationships may be useful as diagnostic tools for climate models and for the eventual understanding of the underlying mechanisms of these associations. The composite fields presented can be used as an indicator of the general condition of the Antarctic ice cover during different phase of the Southern Oscillation as measured by the SOI. We have used these fields to explain, in a broad sense, the large-scale trends and anomalies (reported in recent literature) in the sea ice extent and the length of the ice seasons over the past 20 years. These composite fields are weighted by four strong ENSO episodes over the last 17 years. As a result, these warm events have probably weighted the sea ice and climate anomalies towards the patterns associated with the negative extremes of the SO index. Data of monthly anomalies of ice extent, ice area, and concentration in the Bellingshausen–Amundsen Sea sector (Fig. 9) show that the ice cover in the region is still declining while those in other regions appear to be increasing slightly. In fact, the mean trend of the Antarctic sea ice edge is close to zero over the period. Recession of the ice edge in the Bellingshausen–Amundsen Sea sector is compensated by expansion in the Weddell Sea and western Ross Sea sectors. Our analysis shows that spatially, the Pacific sector is different from other Antarctic regions in that it is influenced by climate anomalies with strong associations with the Southern Oscillation. The results suggest that the Bellingshausen–Amundsen Sea area is unique in its close association with the Southern Oscillation.

*Acknowledgments.* We wish to thank Ian Simmonds and an anonymous reviewer for their valuable comments, especially their suggestions of better procedures to estimate the confidence levels of the observed correlations. The software support provided by S. Pang during the course of this study is appreciated. The SMMR and SSM/I brightness temperature and ice concentration fields are provided by the World Data Center A for Glaciology/National Snow and Ice Data Center (NSIDC), University of Colorado, Boulder, Colorado. Kwok performed this work at the Jet Propulsion Laboratory (JPL) California Institute of Technology under contract with the National Aeronautics and Space Administration.

#### REFERENCES

- Bonekamp, H., A. Sterl, and G. J. Komen, 1999: Interannual variability in the Southern Ocean from an ocean model forced by European Centre for Medium-Range Weather Forecasts reanalysis fluxes. *J. Geophys. Res.*, **104** (C6), 13 317–13 331.
- Carleton, A. M., 1988: Sea ice-atmosphere signal of the Southern Oscillation in the Weddell Sea, Antarctica. *J. Climate*, **1**, 379–388.
- Comiso, J. C., 2000: Variability and trends in Antarctic surface temperatures from in situ and satellite infrared measurements. *J. Climate*, **13**, 1674–1696.
- Ebisuzaki, W., 1997: A method to estimate the statistical significance of a correlation when the data are serially correlated. *J. Climate*, **10**, 2417–2453.
- Gloersen, P., 1995: Modulation of hemispheric sea ice cover by ENSO events. *Nature*, **373**, 503–506.
- Jacobs, S. S., and J. C. Comiso, 1993: A recent sea-ice retreat west of the Antarctic Peninsula. *Geophys. Res. Lett.*, **20**, 171–174.
- , and —, 1997: Climate variability in the Amundsen and Bellingshausen Seas. *J. Climate*, **10**, 697–709.
- Kalnay, E., and Coauthors, 1996: The NCEP/NCAR 40-Year Reanalysis Project. *Bull. Amer. Meteor. Soc.*, **77**, 437–471.
- Karoly, D. J., 1989: Southern Hemisphere circulation features associated with El Niño–Southern Oscillation. *J. Climate*, **2**, 1239–1252.
- King, J. C., and S. A. Harangozo, 1998: Climate change in the western Antarctic Peninsula since 1945: Observations and possible causes. *Ann. Glaciol.*, **27**, 571–575.
- Kwok, R., A. Schweiger, D. A. Rothrock, S. Pang, and C. Kottmeier, 1998: Sea ice motion from satellite passive microwave imagery assessed with ERS SAR and buoy motions. *J. Geophys. Res.*, **103** (C4), 8191–8214.
- Ledley, T. S., and Z. Huang, 1997: A possible ENSO signal in the Ross Sea. *Geophys. Res. Lett.*, **24**, 3253–3256.
- Manabe, S., R. J. Stouffer, M. J. Spelman, and K. Bryan, 1991: Transient responses of a coupled ocean–atmosphere model to gradual changes of atmospheric CO<sub>2</sub>. Part I: Annual mean response. *J. Climate*, **4**, 785–818.
- Mo, K. C., and G. H. White, 1985: Teleconnections in the Southern Hemisphere. *Mon. Wea. Rev.*, **113**, 22–37.
- Parkinson, C. L., 1998: Length of the sea ice season in the Southern Ocean, 1988–1994. *Antarctic Sea Ice: Physical Processes, Interaction and Variability*, M. Jeffnes, Ed., Antarctic Research Series, Vol. 74, Amer. Geophys. Union, 173–186.
- Peterson, R. G., and W. B. White, 1998: Slow oceanic teleconnections linking the Antarctic Circumpolar Wave and the tropical El Niño–Southern Oscillation. *J. Geophys. Res.*, **103** (C11), 24 573–24 583.
- Philander, S. G., and E. M. Rasmusson, 1985: The Southern Oscillation and El Niño. *Advances in Geophysics*, Vol. 28A, Academic Press, 197–215.
- Reynolds, R. W., and T. M. Smith, 1994: Improved global sea surface temperature analyses using optimal interpolation. *J. Climate*, **7**, 929–948.
- Schlesinger, M., and J. Mitchell, 1985: Model projections of the equilibrium climatic response to increased carbon dioxide. *The Potential Climatic Effects of Increasing Carbon Dioxide*, DOE/ER-0237, M. C. MacCracken and F. M. Luther, Eds., U.S. Dept. of Energy, 81–148.
- Simmonds, I., and T. H. Jacka, 1995: Relationships between the interannual variability of Antarctic sea ice and the Southern Oscillation. *J. Climate*, **8**, 637–647.
- Venegas, S. A., M. R. Drinkwater, and G. Shaffer, 2001: Coupled oscillations in Antarctic sea ice and atmosphere in the South Pacific Sector. *Geophys. Res. Lett.*, **28**, 3301–3304.
- Watkins, A. B., and I. Simmonds, 2000: Current trends in Antarctic sea ice: The 1990s impact on a short climatology. *J. Climate*, **13**, 4441–4451.
- White, W. B., and R. G. Peterson, 1996: An Antarctic circumpolar wave in surface pressure, wind, temperature and sea ice extent. *Nature*, **380**, 699–702.
- Yuan, X., and D. G. Martinson, 2000: Antarctic sea ice extent variability and its global connectivity. *J. Climate*, **13**, 1797–1717.